Int J Adv Manuf Technol (2016) 86:799–808
DOI 10.1007/s00170-015-8218-4

ORIGINAL ARTICLE

Simulation-based evaluation of surface micro-cracks and fracture toughness in high-speed grinding of silicon carbide ceramics

Yao Liu [1,2] · Beizhi Li [1] · Chongjun Wu [1] · Yihao Zheng [2]

Received: 2 August 2015 / Accepted: 7 December 2015 / Published online: 28 December 2015

Abstract Surface/subsurface crack during grinding limits the application of engineering ceramics. High-speed grinding is proposed in ceramics grinding for high material removal rate and surface quality. The dynamic fracture toughness of ceramic materials is established by combining the Johnson-Holmquist 2 damage model for brittle material and the Griffith fracture theory. Single-grit simulation was utilized to investigate the individual crack generation and propagation in silicon carbide (SiC) indentation and engagement under different wheel surface speed. The indentation simulation results indicate that high-speed grinding enhances the SiC plastic deformation in the contact zone. Engagement simulation shows that the micro-crack transforms from deep and narrow longitudinal crack in the subsurface to shallow and width lateral crack on the surface when the wheel surface speed increases with a constant maximum undeformed chip thickness. To validate this model, the high-speed grinding experiments are conducted. The trends of micro-crack evolution, single grit force, and surface roughness of the experimental results at the constant workpiece feed rate match well with the simulation results.

Keywords Ceramic · Micro-crack · Dynamic fracture toughness · High-speed · Surface quality

1 Introduction

Grinding of engineering ceramics is challenging in machining efficiency and surface quality. Engineering ceramics are brittle materials widely used in aerospace, precision machinery, and inertial guidance for low density, chemical stability, and high hardness. In ceramics grinding, cracks generate due to the material brittleness and hardness. Cracks result in strength degradation and failure of the ceramic parts [1, 2].

Extensive research has been done to study the crack generation and propagation in ceramic grinding. Zhang et al. [3] observed the grinding-induced cracks in the ceramic and characterized the cracks with three destructive inspection techniques. Agarwal and Rao [4–8] analyzed the damage mechanism in silicon carbide ceramics (SiC) grinding. Wei et al. [9] evaluated the surface micro-cracks in engineering ceramics.

Facture toughness is critical to determine the maximum depth of ductile cutting without micro-crack for ceramic materials with both brittle and ductile removal states. Bifano et al. [10] established a brittle-to-ductile transition formula, where the threshold value is proportional to the material static fracture toughness, according to Lawn's indentation fracture experiments of brittle materials [11] and Griffith's crack propagation criterion [12]. Chen et al. [13] provided another brittle-to-ductile transition formula by comparing the single grit grinding process with the single grit indentation test and using the indentation fracture and micro-hardness measurement formula. This formula defined the dynamic

✉ Yao Liu
yaoliuz@umich.edu

[1] Department of Mechanical Engineering, Donghua University, Shanghai 201600, China

[2] Department of Mechanical Engineering, University of Michigan, Ann Arbor, MI 48105, USA

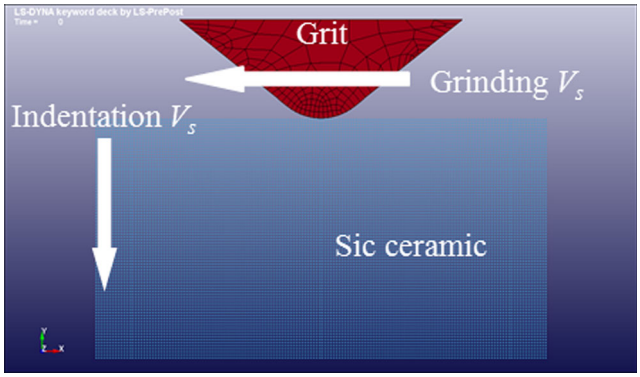

Fig. 1 Schematic for indentation and engagement model

fracture toughness, a constant, K_{ID}, the fracture toughness during machining. Zhu et al. [14] conducted a single-grit high-speed SiC ceramic grinding simulation and determined that the maximum ductile cutting depth is 0.26 μm which is two times larger than the value determined by Bifano et al.

Ceramic has a toughening effect at high stress and strain rate [15–18]. High-speed grinding, with the wheel surface speed of 120 to 200 m/s, generates high stress and strain rate in the grinding zone. The ductile removal process in ceramic grinding, with a sub-micron maximum undeformed chip thickness a_{gmax}, can be significantly affected by the high stress and strain rate.

Missing from the literatures are the micro-crack generation and propagation and fracture toughness in high-speed ceramic grinding and the dynamic fracture toughness model. In this study, the constitutive model, Johnson-Holmquist 2 (JH-2) [15], is applied in the high-speed grinding. A model of K_{ID} is established based on the Griffith's crack propagation criterion. This K_{ID} model is used in a high-speed indentation simulation to predict the ductility of the SiC ceramic. Single-grit engagement simulations are conducted to investigate the high-speed effects on the surface/subsurface cracks and grinding forces. High-speed grinding experiments are conducted to validate the model.

2 Dynamic fracture toughness model

JH-2, obtained from high-speed impact experiments, describes the change of brittle material properties under extreme loading conditions [15–18]. This model is established for ceramics, glass, and other brittle materials under high stress and strain rate. The JH-2 model can be described by the equation below

$$\sigma = \left(1 + C\ln\dot{\varepsilon}\right)\sigma_{\mathrm{HEL}}\left[A\left(\frac{P+T}{P_{\mathrm{HEL}}}\right)^{N} - D\left(A\left(\frac{P+T}{P_{\mathrm{HEL}}}\right)^{N} - B\left(\frac{P}{P_{\mathrm{HEL}}}\right)^{M}\right)\right] \quad (1)$$

where σ is the material equivalent stress under the hydrostatic pressure P and strain rate $\dot{\varepsilon}$. D is the damage degree and T is the maximum tensile hydrostatic pressure the material can withstand. A, B, C, M, and N are constants depending on the material. σ_{HEL} is the equivalent stress at the Hugoniot elastic limit (HEL). P_{HEL} is the pressure at the HEL.

According to the Griffith critical fracture formula [4], the critical fracture stress can be expressed as

$$\sigma_c = \sqrt{\frac{2E\gamma_s}{\pi L(1-\nu^2)}} \quad (2)$$

where L is the length of the material crack, E is the elastic modulus, γ_s is the fracture surface energy, and ν is the Poisson's ratio.

Plastic deformation energy is negligible compared to the fracture surface energy γ_s for brittle materials. γ_s is about a half of the energy release rate when the crack begins to propagate as shown in

$$G_c = K_{IC}^2 / E = 2\gamma_s + \gamma_p \approx 2\gamma_s \quad (3)$$

where K_{IC} is the static fracture toughness.

The critical fracture stress in Eq. (2) can be expressed as

$$\sigma_c = \frac{K_{ID}}{\sqrt{\pi L(1-\nu^2)}} \quad (4)$$

where K_{IC} is substituted by K_{ID} considering the dynamic effects in machining.

Table 1 The material model parameters [14, 30]

Materials	Density (kg/m^3)	Young's modulus (GPa)	Poisson's ratio	Shear modulus (GPa)	Conductivity [W(m K)$^{-1}$]	Specific heat [J/(kg·K)]
SiC	3215	449	0.16	193	180	669.9
Diamond	3560	1000	0.2	–	146.5	502

Assuming the crack initially propagates under the hydrostatic pressure P and strain rate $\dot{\varepsilon}$, the material releases stress via crack propagation in which process the maximum stress is equal to the critical fracture stress σ_c. The dynamic fracture toughness when cracks propagate under load (P, $\dot{\varepsilon}$) can be expressed as

$$K_{ID} = \left(1 + C\ln\dot{\varepsilon}\right)\sigma_{\mathrm{HEL}}\sqrt{\pi L(1\text{-}\nu^2)}\left[A\left(\frac{P+T}{P_{\mathrm{HEL}}}\right)^N - D\left(A\left(\frac{P+T}{P_{\mathrm{HEL}}}\right)^N - B\left(\frac{P}{P_{\mathrm{HEL}}}\right)^M\right)\right] \quad (5)$$

From this equation, the dynamic fracture toughness is determined by material properties and loading conditions including the strain rate, hydrostatic pressure, and damage degree.

3 Numerical simulation

Finite element method (FEM) will be used to simulate the high-speed indentation [14, 19, 20]. Indentation and Hopkinson bar tests are the most commonly used experimental methods to determine the fracture toughness of brittle materials [21–23]. Conventional indentation test cannot measure material high-speed dynamic properties. The Hopkinson bar test can create a high-speed dynamic compression, though the result is of poor accuracy due to the inertial effect [24, 25]. The indentation depth can hardly be controlled in the Hopkinson tests.

The dynamic fracture toughness under different indentation speeds can be characterized by the critical depth of the crack generation, d_c, observed in the FEM, because d_c is proportional to the material fracture toughness [10, 13]. To relate the indentation results to the high-speed grinding, single grit engagement is required because the loading directions are different in indentation and grinding.

The simulation is conducted in LS-DYNA (Livermore Software Technology Corporation (LSTC), US). As illustrated in Fig. 1, the abrasive is modeled as a rigid cone with 116° apex angle. The workpiece is an $8\times4\times0.5$ μm^3 box meshed by smoothed particle hydrodynamics (SPH). All surface particles are constrained by SPH_SYMMETRY_PLANE (SSP) [26–28] except the ground surface. The unit system in this simulation is μg-μm-μs-GPa-mN-nJ. Tables 1 and 2 list the parameters of material property and the JH-2 model, respectively. The erosion criterion is introduced to estimate the material failure due to excessive tensile or compression pressure, based on the total plastic strain. Elements are eroded when the plastic strain exceeds the specified value (FS). Damage occurs when the stress exceeds the material strength, leading to an increment of plastic strain. The material strength is calculated in Eq. (4) by using the dynamic fracture toughness according to the current hydrostatic pressure, strain rate, and damage degree.

The indentation and engagement models are different in grit moving directions as illustrated in Fig. 1. The diamond grit moves vertically in indentation and horizontally from right to left in engagement. Table 3 lists the process parameters of the simulation. The results are interpreted in LSPP (LSTC, US). The indentation force versus depth provides the threshold depth for the crack initiation. The crack width and depth and the force are obtained from the engagement simulations.

3.1 Indentation results and discussion

Figure 2 shows the stress and plastic strain at the indentation speed of 1 m/s. The material undergoes elastic deformation with the grit indentation depth smaller than 0.105 μm. Wave-like stress distribution forms surrounding the indenter (Fig. 2(a-1)). No plastic strain is observed (Fig. 2(b-1)). The material undergoes plastic deformation with the indentation depth between 0.105 and 0.126 μm. Stress concentrates beneath the indenter (Fig. 2(a-2)) with a sharp gradient. Plastic deformation occurs under the indenter without crack (Fig. 2(b-2)). Radial crack generates with the indentation depth larger

Table 2 The JH-2 model parameters for SiC [14–16, 28]

Parameter	ρ_0 (kg/m^3)	G (GPa)	A	N	B	M	C	K_1 (GPa)
Value	3215	193	0.96	0.65	0.35	1.0	0.009	220
Parameter	K_2 (GPa)	K_3 (GPa)	ε_0	T (GPa)	$\sigma^i_{\max}$ (GPa)	$\sigma^f_{\max}$ (GPa)	HEL (GPa)	P_{HEL} (Gpa)
Value	361	0	1.0	0.75	12.2	1.3	11.7	5.13
Parameter	B	D_1	D_2	FS	Damage			
Value	1.0	0.48	0.48	0.2	0			

Table 3 The process parameters

Indentation test		Single grit engagement	
V_S (m/s)	Indentation depth (μm)	V_S (m/s)	a_{gmax} (μm)
1, 10, 20, 80, 100, 120, 140	0.3	20, 40, 80, 100, 140	0.1, 0.15, 0.2, 0.25, 0.3, 0.4, 0.5

than 0.126 μm. Cracks generate in 40° angle with respect to the surface. No median crack is observed. The stress distributes along the cracks (Fig. 2(a-3)). The plastic strain concentrates on the surface and the tip of the crack. This phenomenon agrees with Holmquist et al.'s experimental results [14–16].

Figure 3 shows the abrasive normal force, F_n, at 1 m/s loading speed. The grit contacts with the workpiece at 0.027 μm, followed by the linear increases of F_n due to the workpiece elastic deformation from 0.027 to 0.105 μm indentation depth. F_n fluctuates when plastic deformation occurs with the indentation depth from 0.105 to 0.120 μm. F_n drops sharply when cracks generate with the indentation depth greater than 0.120 μm. F_n bounces back when the indentation depth further increases to crush the debris. In this simulation, the critical depth of SiC indentation cracks is calculated as 0.120–0.027=0.093 μm close to Bifano's critical cutting depth model [10] with the critical crack depth of 0.0891 μm (H=21 GPa, E=449 GPa, K_{IC}=3.5 MPa m$^{(1/2)}$).

Figure 4 presents F_n and the length of each deformation stage at different loading velocities. As shown in Fig. 4a, the elastic modulus (the slope of F_n in the elastic deformation stage) increases with the elevation of V_S. With the increases of V_S from 0.1 to 140 m/s, the length of plastic deformation (red line in Fig. 4b) increases with the increase from 0.012 to 0.1165 μm due to the plastic reinforced effects, the length of elastic deformation (black line in Fig. 4b) decreases by 23 %,

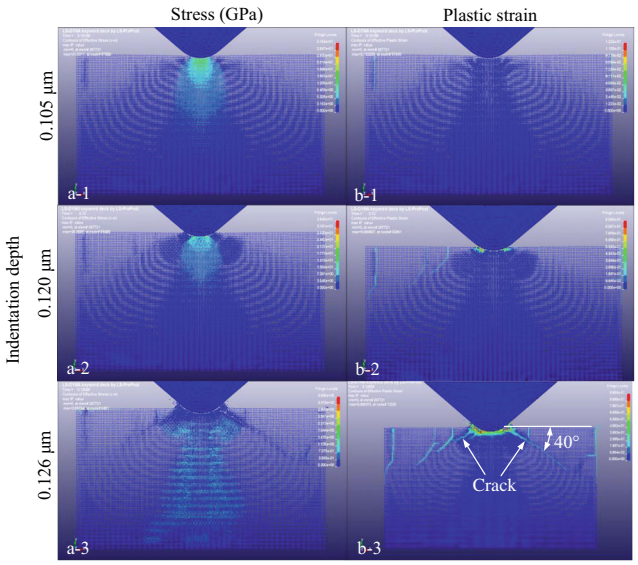

Fig. 2 Crack generation process in indentation with 1 m/s loading speed

and the brittle-to-ductile critical depth (elastic deformation depth + plastic deformation depth) increases. The toughness of the SiC ceramic is enhanced by the high-speed indentation.

3.2 Single-grit engagement result and discussion

The surface and subsurface morphology after engagement at a_{gmax}=0.5 μm is shown in Fig. 5. The maximum widths and depths of cracks, marked as $W_{max(C)}$ and $D_{max(C)}$, respectively, are measured. Grinding is in the ductile mode when the grit passes through at 20 m/s V_S except for the generation of a deep longitudinal crack in the subsurface. This crack is measured as 1.03 μm $W_{max(C)}$ and 3.5 μm $D_{max(C)}$. This subsurface crack degrades the strength and corrosion resistance of the workpiece and induces fatigue failure [21]. $D_{max(C)}$ decreases to 2.56 μm at the increased V_S of 40 m/s. A lateral crack with an increased $W_{max(C)}$ of 3.144 μm generates. The longitudinal crack disappears, and the lateral crack expands to 4.02 μm $W_{max(C)}$ and 0.82 μm $D_{max(C)}$, when V_S is increased to 80 m/s. The proportion of ductile to brittle cutting further decreases when the wheel surface speed reaches 100 m/s and the lateral crack on the surface grows to $W_{max(C)}$=5.08 μm. The surface is covered by shallow lateral cracks without any longitudinal ones, when the wheel surface speed is 140 m/s.

Figure 6 shows the varying crack depth and width at different wheel surface speed. When grinding the SiC at 140 m/s, the crack depth in subsurface reduces to 16 % and the width is enlarged by 6.6 times relative to the 20 m/s, which will enhance the fatigue lifetime of the workpiece and increase the removal rate of the material. For $W_{max(C)}$, the width of crack increases linearly with the increasing speed, while the $D_{max(C)}$

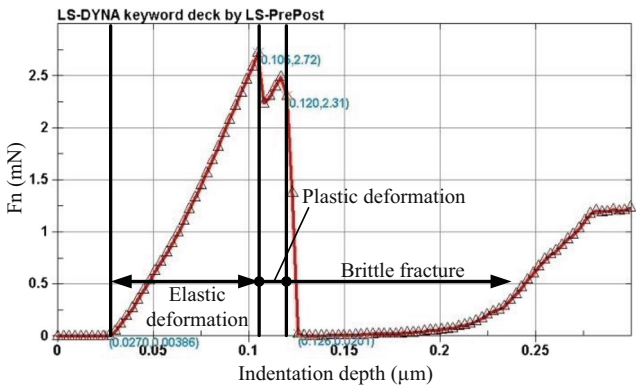

Fig. 3 Normal force, F_n, as a function of the indentation depth at 1 m/s loading speed

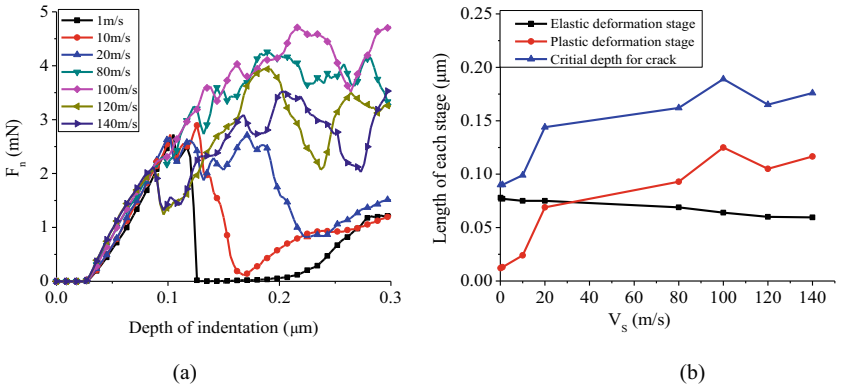

(a) (b)

Fig. 4 **a** F_n and **b** the length of each stage as a function of indentation depth at different V_s

shows bilinear decreasing, which indicates that there is an optimal speed for the grinding of SiC. With the increase of the wheel surface speed, the generation and propagation of the longitudinal cracks are gradually reduced until longitudinal cracks disappear, indicating that the fracture toughness of the workpiece is gradually increasing. While the expansion of the workpiece surface lateral cracks is intensified for the role of the high-speed impact affection, the tangential impaction prompts lateral crack propagation, and thereby making material easy to remove. This finding gives a possibility to suppress generation and propagation of cracks in the longitudinal direction and to promote the material removal process by increasing the speed of the wheel in the actual grinding process. This operation can improve the workpiece subsurface quality to extend its fatigue life and help to remove the material.

Figure 7 illustrates that relationship between engagement force and cutting depth at different wheel surface speeds. The normal forces and tangential forces increase immediately when the a_{gmax} increases. While $a_{gmax} \leqq 0.25$ μm, the variation of forces with the wheel surface speed is not obvious. However, when $a_{gmax} > 0.25$ μm, the effects of high speed on the forces are enhanced. The forces at 20 and 80 m/s increase about 100 and 60 % compared to that at 100 m/s under $a_{gmax}=0.5$ μm. When the material is removed in a ductile mode ($a_{gmax} \leqq 0.25$ μm), increasing the fracture toughness of the workpiece in grinding zone due to the high wheel surface speed will not change the removal mechanism and the force will not be significantly affected by the high speed. The whole single grit engagement is still dominated by ductility, and there is no occurrence of brittle fracture. When a_{gmax} is larger than 0.30 μm and the workpiece undergoes the process of brittle fracture, the engagement force shows differences at various speeds. This demonstrates that high speeds lead to material toughening and significant decline in forces.

This engagement simulation demonstrates that the wheel surface speed influences the strain rate acting on the material and therefore reinforces the dynamic fracture toughness in the contact zone. The critical indentation depth for crack generation can be extended by high speeds. Thus, it can be concluded that the crack generation and propagation can be suppressed by elevating the wheel surface speed. In high-speed machining of ceramics, the cutting depth can be increased relative to the depth at low speeds to improve the material removal rate while attaining a similar or improved surface quality. Therefore, the high-speed machining will be a feasible way to achieve both efficiency and quality of ceramic machining.

4 Experimental validation

The grinding process uses multiple abrasives to cut the workpiece at the same time. It is not reasonable to simply use a

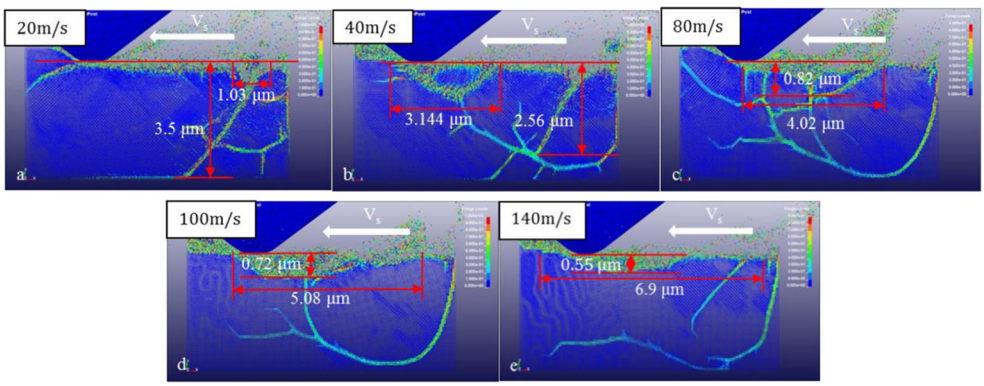

Fig. 5 The surface and subsurface morphology after grinding at $a_{gmax}=0.5$ μm

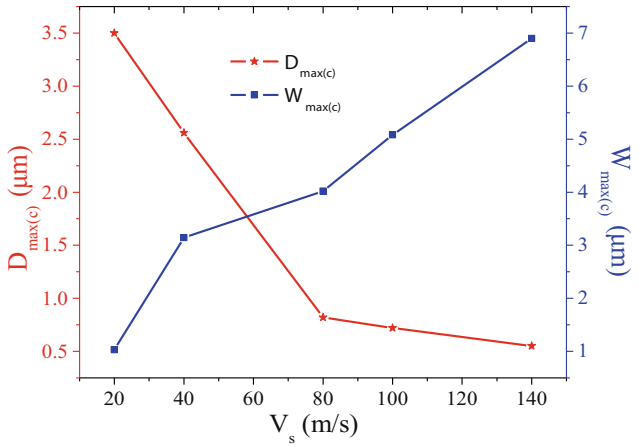

Fig. 6 The variation of longitudinal crack depth and lateral crack width with the wheel surface speed at a_{gmax}=0.5 μm

single grit engagement process to replace the whole wheel grinding process. The grinding process is synthesized by linearly superimposing the function of a single grit and allowing a single grit engagement process to reflect the trends of the entire wheel grinding process. Thus, the results obtained from single grit engagement can be used to predict the whole wheel grinding process trend.

4.1 Experimental methods

The reactive sintering silicon carbide ceramics with 50 μm average particle size are used in this study. As shown in Fig. 8a, SiC workpieces (∅60 mm×20 mm) are made into the cylindrical ring. The grinding experiments will be conducted on the outer surface of the ring. In order to check the subsurface crack, each SiC workpiece is made into two parts. Each contacted subsurface will be roughly polished by 20, 10, 5, and 2 μm diamond abrasive for an hour, and then the 0.5 μm abrasive will be used to fine polish the contacted subsurface for more than 3 h. The contacted subsurface is used to observe the crack in the subsurface and will not be ground in these experiments. The SiC is mounted on the workpiece shaft. Before the experiments, all ground surfaces will be pre-ground ten times under V_s=100 m/s, V_w=0.1 m/s, a_p= 0.1 μm, and then sparking out ground for 3 min. The experiment setup is given by Fig. 8b. The CNC cylindrical grinder (MGKS1332/H) is used to conduct the experiments. The tool is a vitrified diamond grinding wheel (Winter, Swiss) with the dimension of ∅400 mm×15 mm. The average grit size is 91 μm. An SBS balancing instrument is embedded in the motor spindle to make the unbalance under 0.02 μm before each test. Dynamometer (Kistler 9123C) is installed on the workpiece axis to measure the grinding forces. In order to eliminate the effects of wheel wear, the wheel is dressed by the diamond wheel every five experiments.

Experimental parameters are listed in Table 4. In the cylindrical grinding process, the a_{gmax} cannot be controlled directly. In order to ensure that the a_{gmax} remains unchanged, one or both of V_W and depth of cut a_p should be changed as the V_S is increased. The five tests are divided into two groups and marked as group 1 (a_p is constant, changing the V_S and V_W at the same time to make sure the a_{gmax} always same) and group 2 (V_W is constant, changing the V_S and a_p simultaneously to keep the a_{gmax} unchanged), to discuss the high-speed grinding process at the same a_{gmax}. In order to discuss the grinding efficiency later, the material removal rate is defined as:

$$Q_w' = V_w a_p \tag{6}$$

Five SiC samples are used in this experiment, since test 2 in groups 1 and 2 has the same grinding parameters. Each sample is ground five times to measure the force and surface roughness (R_a) (using the 3D optical profilometer (NPFLEX)). After the total 25 experiments are completed, the average force and R_a are extracted. After all measurements are finished, those quarter ring SiC samples are eroded by the concentrated nitric (HNO_3) and hydrofluoric (HF) acid to make the cracks more visible. The cracks on the ground surface and contacted subsurface are imaged with a scanning electron microscope (SEM). The maximum crack size in the whole surface and subsurface is measured.

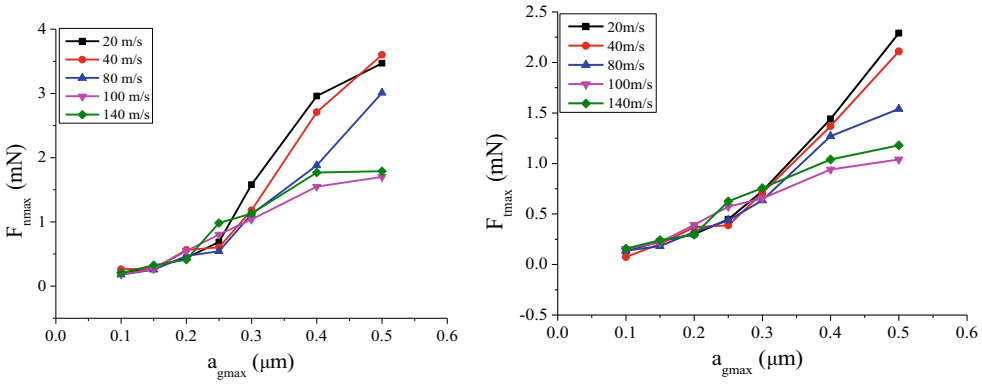

Fig. 7 The influence of a_{gmax} on force at V_s=20, 40, 80, 100, and 140 m/s

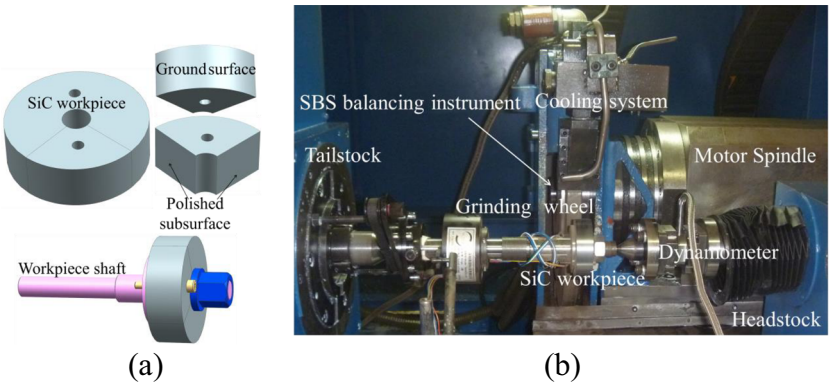

Fig. 8 **a** SiC workpiece setup and **b** experiments setup

4.2 Experiments results

The ground surface is investigated by SEM as shown in Fig. 9. Cracks are identified with white outlines. Within group 1, the crack size increases, the number of cracks decreases, and the crack depth shows no difference, when V_s increases from 20 to 80 and 140 m/s, as can be observed in Fig. 9a, 1, 2, and 3, respectively. Increasing V_s leads to the crack extension and connection on a same subsurface. Group 2 shows the similar trends in crack size and quantity. Within group 2, the cracks at low V_s are deep and penetrate into the subsurface in a larger angle with respect to the workpiece surface. The ductile grinding zone area shrinks while increasing the V_s. This observed crack propagation mechanism in group 2 matches well with the engagement simulation.

Figure 10 shows the typical micrographs of the contacted subsurface after grinding. Groups 1 and 2 demonstrate the decrease of cracking depth as wheel surface speed is increased. In group 1, the crack depth reduced from 95 to 55 μm and 34 μm as wheel surface speed is increased from 20 to 80 m/s and 140 m/s, respectively. As for group 2, the decrease in crack size is more significant compared to group 1. As the wheel surface speed is increased from 20 to 80 m/s and 140 m/s, a proportion of 83 % decrease on crack length is observed with cracks measuring 140, 55, and 23 μm, respectively. The reduction of the crack depths exhibits the increase of material K_{ID} in the grinding zone. As the wheel surface speed is increased and the material becomes more ductile, stress concentration is dispersed and crack propagation is suppressed. The decrease in crack depth will improve the surface integrity impressively. Experimental crack depth trends in subsurface fit well with the simulation results, which verifies the validity of the simulation.

Figure 11 shows the experimental results, including the average force, surface roughness, and material removal rate. In group 1 (Fig. 11a), though the material removal rate increased about 700 % from 0.075 mm^3/mm s at 20 m/s to 0.525 mm^3/mm s 140 m/s, the single grit force remains constant. Since the grinding zone material strain rate $\dot{\varepsilon}$ increased with increasing V_S, the K_{ID} also increased according to Eq. (5). This results in a decrease in surface roughness from 0.41 to 0.28 μm. For group 2 (Fig. 11b), when the wheel surface speed is increased, K_{ID} also increased due to the high strain rate which caused the material to become "soft" and therefore decreased the friction force [14, 29] to decrease single grit grinding force. Even a substantial increase, up to 4500 %, in material removal rate is observed in this group. Considering the surface roughness, as the cracks do not propagate to the surface in low-speed, the surface only had some tiny holes and most of the ground surface undergo ductile ground and therefore resulted in an a small R_a value. When the wheel surface speed increased to 80 m/s, the cracks that propagate to the surface can connect with each other. This enables the cracks on the surface to become larger, and therefore the R_a measured is larger than the R_a observed at 20 m/s. In contrast, at 140 m/s, the cracks became shallower which decreased the R_a even with enlarged crack widths. The force and surface roughness in the single grit simulation are also constant with group 2.

When the grinding wheel surface speed increased, the crack depths decreased regardless of whether the single grit force decrease or remain constant which means the material become tougher. Comparing the experiments test 1 and test 3 in group 1 with test 1 and test 3 in group 2, the workpiece material suffered the same strain rate for the same wheel surface speed. Test 1 in group 2 and test 3 in group 1 show deeper crack size than that of test 1 in group 1 and test 3 in group 2

Table 4 Grinding process

	Test	V_S (m/s)	V_W (m/s)	a_p (μm)	a_{gmax} (μm)
Group 1	1	20	0.025	3	0.52
	2	80	0.1	3	0.52
	3	140	0.175	3	0.52
Group 2	1	20	0.1	0.2	0.52
	2	80	0.1	3	0.52
	3	140	0.1	9.1	0.52

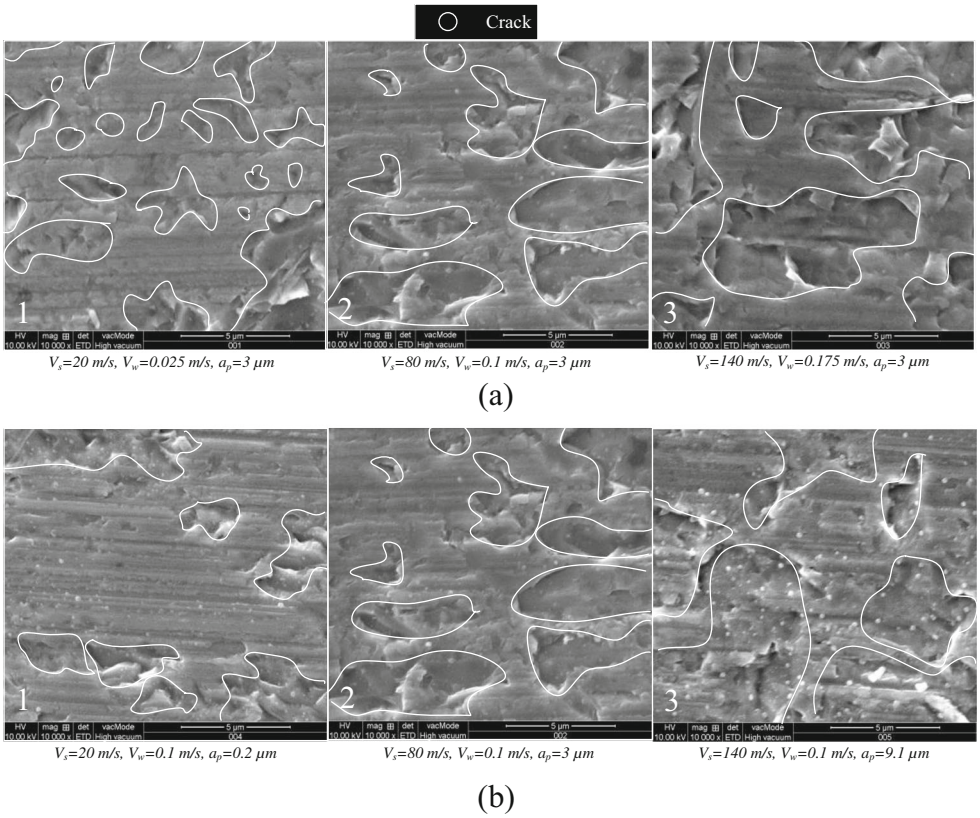

Fig. 9 SEM observation of ground surface after grinding (×10000). **a** Group 1 and **b** group 2

due to the larger grinding force. Improving the material strain rate and lowering single grit grinding forces can reduce subsurface cracks significantly and improve the grinding quality of the workpiece. Considering the ground surface, group 2 shows fewer cracks in low-speeds and shallower cracks at high-speeds. The crack depth descent rates of test 1 to test 3

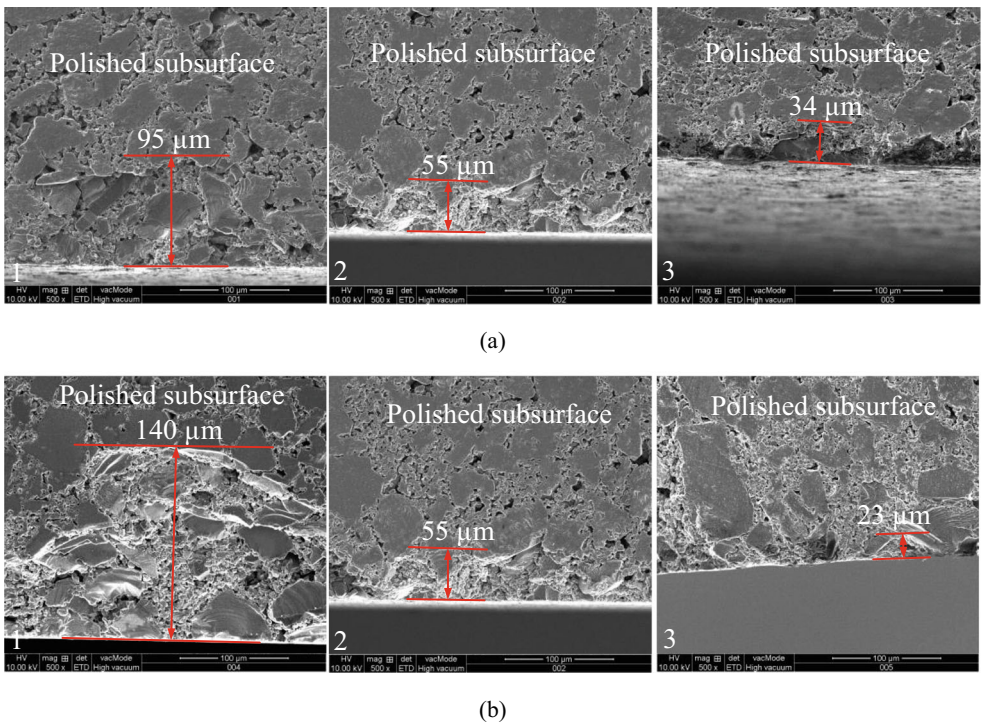

Fig. 10 SEM observation of polished subsurface after ground (×500). **a** a_p=0.3 μm, V_S/V_W=800, a_{gmax}=0.52 μm and **b** V_W=0.1 m/s, a_p=0.2, 3, 9.1 μm, a_{gmax}=0.52 μm

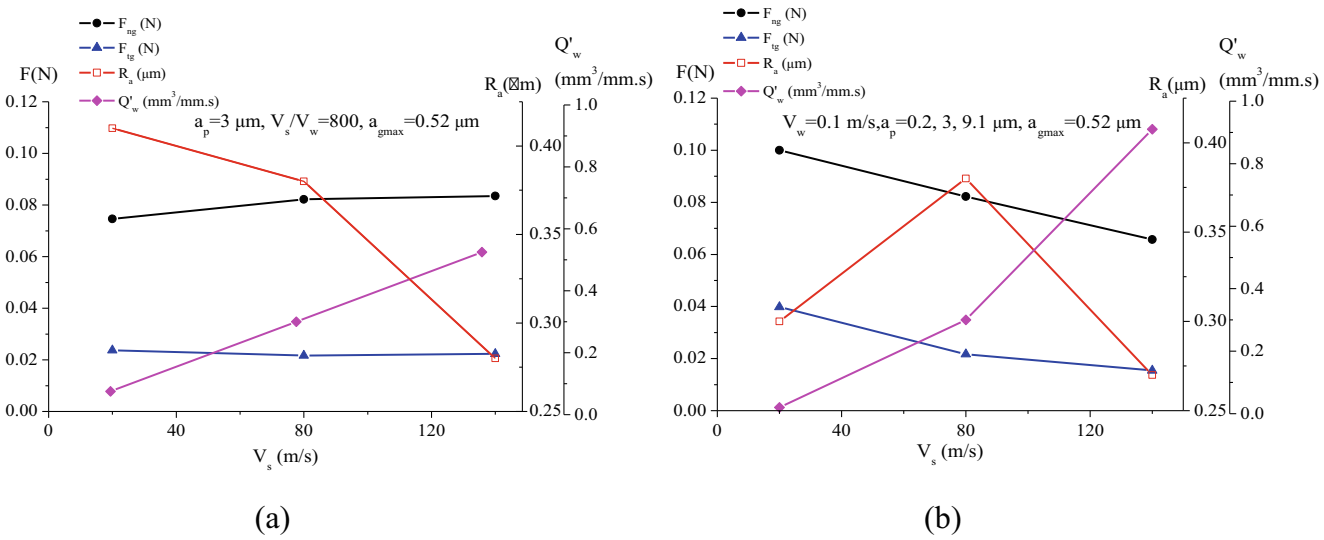

Fig. 11 Grinding force, surface roughness, and material remove rate as a function of grinding wheel surface speed at the a_{gmax}=0.52 μm. **a** Group 1 and **b** group 2

in group 2 are faster than that of test 1 to test 3 in group 1. Indicating that elevating a_p is more efficient to improve subsurface quality compared to elevating V_W in high-speed grinding. This means that the a_p mainly affects the crack depth generation and propagation on the subsurface while the V_w affects the crack generation and propagation on the surface. Thus, the combination of high-speeds, large cutting depths, and low feed rates can greatly improve the material removal rate while maintaining or reducing the crack depth, ultimately leading to efficient and high-quality grinding.

All the simulation results, regardless of the force, surface roughness, surface or subsurface crack, are consistent in trends with experiments in group 2, which are verified with the simulation model and dynamic fracture toughness model. As for group 1, the simulation model requires improvement to discuss the high-speed effect at the constant speed rate of V_s/V_w.

5 Conclusions

Dynamic fracture toughness and fracture mechanism in SiC high-speed grinding are investigated by SPH&FE simulation and experiments.

(1) The dynamic fracture toughness of the ceramic materials in high-speed machining is affected by strain rate, hydrostatic pressure, and material damage degree.
(2) The elevated wheel surface speed enhances the SiC dynamic fracture toughness. This enlarges the lateral and shrinks the longitudinal cracks on the workpiece and reduces the grinding force.
(3) The high-speed grinding can achieve high material removal rates with better surface and subsurface quality in SiC ceramic machining.

References

1. Li K, Liao TW (1996) Surface/subsurface damage and the fracture strength of ground ceramics. J Mater Process Technol 57:207–220
2. Rao PV, Agarwal S (2005) A new surface roughness prediction model for ceramic grinding. Proc Inst Mech Eng B J Eng Manuf 219(11):811–819
3. Zhang B, Zheng XL, Tokura H, Yoshikawa M (2003) Grinding induced damage in ceramics. J Mater Process Technol 132(1–3): 353–364
4. Agarwal S, Rao PV (2008) Experimental investigation of surface/subsurface damage formation and material removal mechanisms in SiC grinding. Int J Mach Tools Manuf 48(6):698–710
5. Agarwal S, Rao PV (2010) Grinding characteristics, material removal and damage formation mechanisms in high removal rate grinding of silicon carbide. Int J Mach Tools Manuf 50(12):1077–1087
6. Agarwal S, Rao PV (2012) Predictive modeling of undeformed chip thickness in ceramic grinding. Int J Mach Tools Manuf 56: 59–68
7. Agarwal S, Rao PV (2010) Modeling and prediction of surface roughness in ceramic grinding. Int J Mach Tools Manuf 50(12): 1065–1076
8. Agarwal S, Rao PV (2013) Predictive modeling of force and power based on a new analytical undeformed chip thickness model in ceramic grinding. Int J Mach Tools Manuf 65:68–78
9. Wei S, Zhao H, Jing J, Liu Y (2015) Investigation on surface microcrack evaluation of engineering ceramics by rotary ultrasonic grinding machining. Int J Adv Manuf Technol 81:483–492
10. Bifano TG, Dow TA, Scattergood RO (1991) Ductile regime grinding: a new technology for machining brittle materials. J Eng Ind 113:184–189

11. Lawn BR, Wilshaw TR (1993) Fracture of brittle Solids. Cambridge University Press: 143–375
12. Lawn BR, Wilshaw TR (1993) Fracture of brittle solids. Cambridge University Press: 1–14
13. Chen M, Zhao Q, Dong S, Li D (2005) The critical conditions of brittle–ductile transition and the factors influencing the surface quality of brittle materials in ultra-precision grinding. J Mater Process Technol 168(1):75–82.7
14. Zhu D, Yan S, Li B (2014) Single-grit modeling and simulation of crack initiation and propagation in SiC grinding using maximum undeformed chip thickness. Comput Mater Sci 92:13–21
15. Holmquist TJ, Johnson GR (2005) Characterization and evaluation of silicon carbide for high-velocity impact. J Appl Phys 97(9): 093502.1–093502.12
16. Holmquist TJ, Johnson GR (2002) Response of silicon carbide to high velocity impact. J Appl Phys 91(9):5858–5866
17. Johnson GR, Holmquist TJ (1994) An improved computational constitutive model for brittle materials. J Appl Phys 309:981–984
18. Johnson GR, Holmquist TJ, Beissel SR (2003) Response of aluminum nitride (including a phase change) to large strains, high strain rates, and high pressures. J Appl Phys 94(3):1639–1646
19. Cai MB, Li XP, Rahman M (2007) Study of the mechanism of nanoscale ductile mode cutting of silicon using molecular dynamics simulation. Int J Mach Tools Manuf 47(1):75–80
20. Chuang TJ, Jahanmir S, Tang HC (2003) Finite element simulation of straight plunge grinding for advanced ceramics. J Eur Ceram Soc 23(10):1723–1733
21. Malkin S, Hwang TW (1996) Grinding mechanisms for ceramics. CIRP Ann Manuf Technol 45(2):569–580
22. Evans AG, Charles EA (1976) Fracture toughness determinations by indentation. J Am Ceram Soc 59(7–8):371–372
23. Hopkinson B (1914) A method of measuring the pressure produced in the detonation of high explosive or by the impact of bullets. Philos Trans R Soc London 213:437–456
24. Li YL, Liu YY (1993) Calculation of DSIF of three point bending specimen using the method of DCOD. Explosion and Shock Waves 13(3):249–256
25. Liu RT, Zhang XX, Jiang FC (2000) Analysis of dynamic response of stress intensity factor of three-point bending specimen by using finite element method. Journal of Harbin Engineering University 21(3):49–51
26. Limido J, Espinosa C, Salaun M, Lacome JL (2007) SPH method applied to high speed cutting modelling. Int J Mech Sci 49(7):898–908
27. Xi Y, Bermingham M, Wang G, Dargusch M (2014) SPH/FE modeling of cutting force and chip formation during thermally assisted machining of Ti6Al4V alloy. Comput Mater Sci 84:188–197
28. Duane S, Cronin KB (2002) Implementation and validation of the Johnson–Holmquist ceramic material model in LS-DYNA. 4th European LS-DYNA Users Conference. D-1
29. Li B, Ni J, Yang J, Liang SY (2013) Study on high-speed grinding mechanisms for quality and process efficiency. Int J Adv Manuf Technol 70(5–8):813–819
30. Yuan Y (2012) Experimental research on the mechanism of high-speed grinding for hard and brittle materials, Master thesis, Donghua University